Monthly Notices of the ROYAL ASTRONOMICAL SOCIETY

MNRAS **512,** L27–L32 (2022) https://doi.org/10.1093/mnrasl/slac018
Advance Access publication 2022 February 23

Revealing dual radio sources in a sub-kpc-scale binary active galactic nucleus candidate

J. E. Brooks,[1]★ M. K. Argo ,[1] Hojin Cho ,[2] Jong-Hak Woo,[2] Taehyun Jung[3,4] and N. Wrigley[5]

[1]*Jeremiah Horrocks Institute, University of Central Lancashire, Preston PR1 2HE, UK*
[2]*Department of Physics and Astronomy, Seoul National University, Seoul 08826, Republic of Korea*
[3]*Korea Astronomy and Space Science Institute, Yuseong-gu, Daejeon 34055, Republic of Korea*
[4]*Department of Astronomy and Space Science, University of Science and Technology, 217 Gajeong-ro, 34113, Daejeon, Republic of Korea*
[5]*Jodrell Bank Centre for Astrophysics, School of Physics and Astronomy, The University of Manchester, Manchester, SK11 9DL, UK*

Accepted 2022 February 11. Received 2022 February 9; in original form 2021 September 29

ABSTRACT

We present new imaging of a sub-kpc-scale binary active galactic nucleus (AGN) candidate from the Karl G. Jansky Very Large Array (VLA) and the Multi-Element Radio Linked Interferometer Network (e-MERLIN). Two unresolved radio sources of similar luminosity around 10^{22} WHz^{-1} are identified in ∼35 h of e-MERLIN 6 cm imaging. These radio sources have an angular separation of 0.19 ± 0.06 arcsec and position angle (PA) of $22^{\circ} \pm 10^{\circ}$, corresponding to a projected separation of 0.95 ± 0.29 kpc at the epoch of the source. Our results suggest the presence of a kpc-scale active black hole pair hosted by two galaxies in the late stage of a merger at $z = 0.35$. This work follows Woo et al., which presented two optical sources with a similar separation and PA, and a velocity separation of 200 km s^{-1}. Our target adds to the currently limited sample of close-separation binary AGNs, which will aid in understanding the frequency of mergers and the stochastic gravitational wave background.

Key words: galaxies: active – galaxies: interactions – galaxies: nuclei – radio continuum: galaxies.

1 INTRODUCTION

The exact role of the central supermassive black hole (SMBH) in the evolution of a galaxy is still unclear, but it is clear that mergers between galaxies can have a major impact on the life cycle of a galaxy (Kormendy & Ho 2013). During a merger of two massive gas-rich galaxies, accretion on to one or both of the central SMBHs can be triggered producing a bound pair of active galactic nuclei (AGNs). This merger proceeds in a series of stages before coalescence (Begelman, Blandford & Rees 1980; Colpi 2014; Komossa & Zensus 2016). First, the two galaxies begin their interaction via momentum losses to dynamical friction. This continues until the binary separation is approximately 1 pc, then the pair begins to secure itself and the binary 'hardens'. It is here where our understanding becomes slightly more murky, as the processes that take over dynamical friction to drive the merger may not operate on time-scales that agree with observation. Early models even suggested that the binary can stall for longer than a Hubble time, commonly referred to as the 'final-parsec' problem (Khan, Just & Merritt 2011; Khan et al. 2013; Holley-Bockelmann & Khan 2015; Vasiliev, Antonini & Merritt 2015). Our understanding picks back up again as the binary approaches coalescence and efficient gravitational wave emission takes over to drive the merger to its conclusion. Here, a massive burst of gravitational energy is emitted, which will be clearly detected by observatories like the *Laser Interferometer Space Antenna* (*LISA*; Danzmann et al. 2017).

Studying these mergers is therefore critical to the future of the burgeoning field of gravitational wave astronomy, which can in turn deliver important insights into the entire field of astrophysics. In addition to being a strong source of emission for even our early gravitational observatories, mergers are thought to contribute to a stochastic background signal known as the gravitational wave background (GWB; Goulding et al. 2019). As pulsar timing arrays continue to operate at lower and lower frequencies, so the interest in this field grows (Manchester et al. 2013; Verbiest et al. 2016), and decomposing the relative contributions of various mechanisms to the GWB becomes an active area of research. Quantifying the contribution of binary AGNs to the GWB necessarily requires a large sample of mergers at varying stages to approximate the rate of gravitational wave events. Furthermore, this sample could also be used in studying the galaxy merger process beyond $z \sim 0$, where major mergers seem to have at least partly driven changes in galaxy morphology (Conselice 2014). Therefore, compiling a sample of close-separation binaries provides an important tool for testing future theories and models of galaxy evolution and cosmology. Currently, this sample is quite limited (see e.g. Rubinur, Das & Kharb 2018; De Rosa et al. 2019, for a review), and the sample of close-separation binaries is especially small (e.g. Komossa et al. 2003; Rodriguez et al. 2006; Fu et al. 2015; Kharb, Lal & Merritt 2017; Goulding et al. 2019).

The origin of the radio emission in radio-faint AGNs, like those presented in this Letter, is an ongoing topic of research (see Padovani 2016 for a review). It has been shown that there is a loose correlation of jet power with radio power, such that radio-loud AGNs contain strong jets and radio-weak AGNs contain weak or non-existent

★ E-mail: jebrooks@uclan.ac.uk

jets, and the origin of emission is likely dominated by some other mechanism operating in the host galaxy or the local environment of the central engine (Bonzini et al. 2015; Panessa et al. 2019). This other mechanism is usually star formation; therefore, radio-faint populations are mostly composed of AGNs and star formation dominated sources (Padovani et al. 2015). As is often the case, this is not a global rule. An example of one such exception is the strongly lensed system studied by Hartley et al. (2019), which shows dominant jet emission in a sub-mJy source on scales below a parsec. Identifying the dominant origin of emission in radio-faint AGNs often requires multiwavelength observations and a combination of long- and short-baseline interferometers in the radio.

This Letter presents new evidence for the binary AGN nature of the object SDSS J132323.33−015941.9 using radio imaging from both the Karl G. Jansky Very Large Array (VLA) and the Multi-Element Radio Linked Interferometer Network (e-MERLIN). We will build off the findings of Woo et al. (2014), who first identified the object as a candidate sub-kpc-scale binary AGN through *Hubble Space Telescope* (*HST*) imaging and Very Large Telescope Integral Field Unit (VLT IFU) spectra. They find two stellar cores in the *HST* imaging with an angular separation of 0.20 ± 0.01 arcsec and a position angle (PA) of $12.^{\circ}9 \pm 4.^{\circ}0$. These stellar cores overlap with two velocity components found in the IFU spectra that share very similar spatial separation and PA measurements, along with a velocity separation of $\sim$200 km s^{-1}, typical of a late-stage galaxy merger (Liu et al. 2010). Furthermore, the [O III]/Hβ flux ratio of both components is much larger than 3, indicating that the ionization source of each component is an AGN. Further details of the optical properties of the target can be found in Woo et al. (2014).

The object, hereafter referred to as J132323, is located at $\alpha = 13^{\rm h}23^{\rm m}23.^{\rm s}33$ and $\delta = -01^{\circ}59'41.''9$, with a redshift $z = 0.350280 \pm 0.000014$ as measured in DR13 of the Sloan Digital Sky Survey (Albareti et al. 2017). Assuming $H_0 = 70\,{\rm km\,s^{-1}\,Mpc^{-1}}$, $\Omega_\Lambda = 0.7$, and $\Omega_{\rm m} = 0.3$, 1 arcsec corresponds to 4.94 kpc at the local epoch of J132323. In this Letter, we first present new radio observations of J132323 in Section 2 and our initial analyses in Section 3. The implications of our findings are discussed in Section 4, and we present our conclusions in Section 5.

2 OBSERVATIONS

2.1 VLA observations

The target was observed by the VLA under project code 15A-072 (PI: J. Woo) in both *C* band and *L* band in 2015 July and August, respectively, in A configuration for 10 and 18 min (total on-source time), respectively. The observations were conducted with all available antennas and covered 2.048 GHz around 5.5 GHz for the *C* band and 1.024 GHz around 1.5 GHz for the *L* band. Both observations split up their respective bandwidths into 16 spectral windows of 64 channels. The data products were retrieved from the archive in early 2021 and passed through the VLA pipeline packaged with CASA.[1] No extra flags were applied after the pipeline run.

The VLA observations were successful in detecting a single unresolved source of radio emission in both bands (see Fig. 1). These sources show peaks of 0.236 ± 0.01 mJy beam^{-1} at the *C* band and 1.39 ± 0.03 mJy beam^{-1} at the *L* band. The VLA synthesized beam is 1.3 and 0.33 arcsec at the *L* band and *C* band, respectively; both are around seven times larger than e-MERLIN beam sizes. Therefore, we expect that the VLA will measure greater peak emission values than equivalent measurements from e-MERLIN.

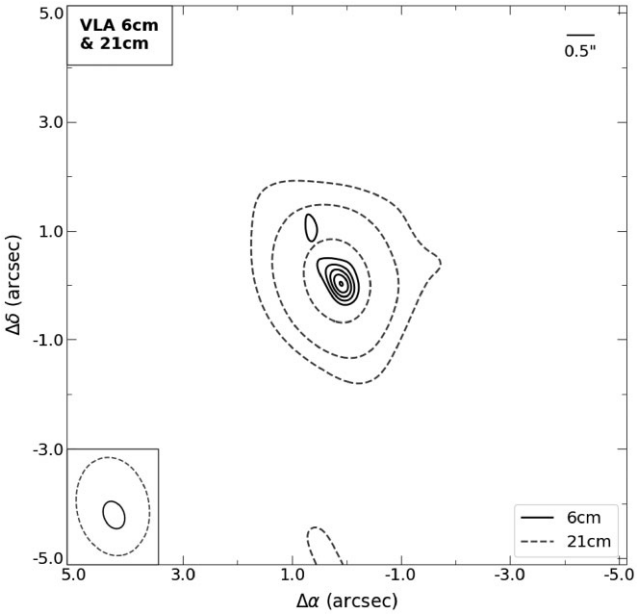

Figure 1. Contours of both the 21 and 6 cm VLA images. Contours for the 21 cm data are given on a logarithmic scale, -3σ, 3σ, 9σ, 27σ,..., where σ is the 21 cm rms noise. Contours for the 6 cm data are given on a linear scale, $-5\sigma, 5\sigma, 9\sigma, 13\sigma$,..., where σ is the 6 cm rms noise. The clean beams used to restore each of the images are given superimposed and to-scale in the bottom left-hand corner. The image shows the initial detection of an unresolved radio source within J132323.

2.2 e-MERLIN observations

Radio imaging of the target was conducted by e-MERLIN over 17 *C*- and *L*-band observations between 2016 November and 2020 September (see Table 1). This totals to $\sim$35 h on-source time at the *C* band (5 GHz/6 cm) and $\sim$8 h on-source time at the *L* band (1.5 GHz/21 cm), with flags applied. All observations utilized all available antennas excluding the Lovell Telescope, giving a maximum baseline of 217 km (Knockin – Cambridge) and a minimum baseline of 11 km (Mk II – Pickmere). The *L*-band spectral range covered 512 MHz centred at 1.51 GHz, broken up into eight spectral windows of 64 MHz each. Each spectral window was averaged to 128 channels of 0.5 MHz. The *C*-band spectral range covered 512 MHz centred at 5.07 GHz, broken up into four spectral windows of 128 MHz each. Each spectral window was also averaged to 128 channels, giving a slightly larger channel width of 1 MHz.

Observations conducted in 2016 were generally of a high quality, though the first *C*-band observation on November 25 is significantly shorter (only 7 h including overheads), making calibration and imaging more difficult. One of the two follow-up observations conducted in 2017 (March 8) suffered critical data loss for unknown reasons and was omitted from the study. In the first two *L*-band observations conducted in 2020, quite a few medium-length baselines were lost due to hardware issues. The *C*-band observations conducted on August 21 and 22 suffered critical data loss due to a combination of very poor weather conditions and hardware problems. These two data sets were also omitted from the study.

[1] see the webpage: https://science.nrao.edu/facilities/vla/data-processing/pipeline

Table 1. A table of all observations of the target conducted by e-MERLIN in the 2016–2020 period. Observations conducted in 2016–2017 are under the project code CY4205 (PI: J. Woo), while observations conducted in 2020 are under CY10204 (PI: M. Argo). The statistics of the total combined visibility data is presented at the bottom. The rms values quoted for the individual *C*-band epochs are measured from the dirty images as no source is detected in these; therefore, no cleaning is appropriate. The on-source time presented is the total integration time on the source with flags applied.

Epoch	Band	On-source time (h)	rms noise (μJy beam^{-1})	Source/s peak (μJy beam^{-1})
2016 Nov 25	*C*	1.6	48	–
2016 Nov 26	*C*	3.4	42	–
2016 Nov 27	*C*	3.6	42	–
2016 Dec 13	*C*	3.9	40	–
2016 Dec 14	*C*	3.9	29	–
2017 Apr 6	*C*	4.8	25	–
2020 Aug 18	*C*	3.5	23	–
2020 Aug 20	*C*	2.5	23	–
2020 Aug 23	*C*	3.2	28	–
2020 Aug 29	*C*	4.5	24	–
2016 Dec 21	*L*	2.9	32	404
2020 Sept 8	*L*	1.3	56	359
2020 Sept 10	*L*	1.0	66	373
2020 Sept 11	*L*	2.9	34	338
All	*C*	34.9	8.7	56/87 (NE/SW)
All	*L*	8.1	22	357

After being passed through the e-MERLIN CASA pipeline,[2] any problematic data such as spurious signals or data from faulty antennas were manually identified and flagged to reinforce the quality of each observation. Image fidelity and point-source response are a particular issue with this target when observing with e-MERLIN, as the maximum elevation of target is only $\sim$35° above the horizon producing an extremely elongated point spread function (PSF). To correct the elongated image artefacts produced by this PSF, we restored the images in Fig. 2 using a circular restoring beam with a full width at half-maximum (FWHM) appropriate to the observing frequency. After flagging, the data were self-calibrated until the rms noise in the outer regions of the image field reached a minimum.

The image produced by each observation was inspected for sources, manually masked, and then cleaned using the standard Högbom algorithm implemented in CASA (Högbom 1974) to a 3σ limit – three times the predicted rms noise. The individual *L*-band observations show a single, clear, unresolved source (see Fig. 2). Note that for some of the *L*-band images, the source appears to be marginally resolved, though the difference between the total flux from the source and the peak flux density is minimal. Furthermore, the large-scale noise structures produced by sparser coverage on medium-length baselines could most certainly distort the central region such that the target falsely appears marginally resolved. Each *C*-band image for a single epoch does not immediately show any signs of a dual source; however, after combining and imaging the visibility data of all *C*-band observations, two distinct radio sources appear above the noise (see Fig. 2).

[2]see the GitHub repository: https://github.com/e-merlin/eMERLIN_CASA_pipeline

3 METHODS AND RESULTS

Positional measurements of the sources apparent in the combined e-MERLIN *C*-band image were performed by first fitting a pair of two-dimensional elliptical Gaussian models. It is important to note here that the fitting was performed on the map that was restored with the circular restoring beam and not the highly elongated clean beam produced by the Högbom algorithm. In the map restored with the clean beam, the two sources blur into one another and make fitting realistic models very difficult. We therefore decided that a more accurate model of the sources could be obtained by fitting to the map created by the idealized circular restoring beam. The angular separation of the centroids of the two models is 0.19 arcsec, with a PA of 22°. We take the fitted sigma value within the Gaussian model as our uncertainty of the centroid position, giving a separation of 0.19 ± 0.06 arcsec and a PA of $22° \pm 10°$. This corresponds to a projected separation of 0.95 ± 0.29 kpc at the epoch of the source. These measurements are similar to the positional measurements of the stellar cores obtained by Woo et al. (2014), suggesting that the unresolved radio emission from sources A and B originates from the centre of the stellar cores. The radio sources are faint when compared to a typical AGN, with 5 GHz luminosities around $\sim 10^{22}$ WHz^{-1} measured with both the VLA and e-MERLIN. This increases slightly to around $\sim 10^{23}$ WHz^{-1} at 21 cm. More specifically, we measure $P_L = 3.1 \pm 0.1 \times 10^{23}$ WHz^{-1} for the VLA and slightly less from e-MERLIN with $P_L = 8.6 \pm 0.5 \times 10^{22}$ WHz^{-1}, both at a distance of 1.38 Gpc at the present epoch.

The temporal sampling of the target is very irregular, so detecting any variability that might give clues as to the spatial scale over which the emission originates is not feasible. We measure a 10 per cent decline in total 21 cm emission in the 4 yr gap between observations, though it is currently impossible to determine if this is due to instrumental errors, or if it is an absolute change, or if we are simply sampling an instant of a periodic fluctuation. It remains a possibility that if the target was detectable in the *C*-band imaging at single epochs, some variability might be accounted for given the frequency of observation. Put simply, these e-MERLIN observations cannot, on their own, reveal any information about source variability. Further radio observations are therefore necessary to investigate this aspect of J132323.

Given that e-MERLIN cannot resolve two sources of 21 cm emission in addition to the 6 cm sources, a spectral index value of an assumed power law is limited in its interpretation. Despite this, we calculate an index of $\alpha = 0.76 \pm 0.14$ (where $S_\nu \propto \nu^{-\alpha}$) by taking the peak flux density of the single *L*-band source and summing the peak flux densities of sources A and B. Note that this approach underestimates the total 6 cm flux that is comparable to the total 21 cm flux, so the quoted index is a slight overestimate. In addition, this method cannot account for any temporal variance of the source, so the index will be an average over the observation epochs. Assuming that sources A and B are similar in nature, the value of α suggests the presence of two approximately flat-spectrum radio sources – commonly associated with AGNs (Padovani et al. 2017). Furthermore, the VLA imaging presents a single radio source with a spectral index of $\alpha = 1.38 \pm 0.06$, suggesting a steeper radio spectrum characteristic of stronger non-thermal emission. We stress though that these indices are based on unsuitable measurements as we know there are two sources of radio emission within J132323; thus, any reliable measurement or comparison of spectral index (or indeed any other attribute) must measure sources A and B separately. A spectral index image of the e-MERLIN 21 and 6 cm data does not show any features of interest. A brightness temperature

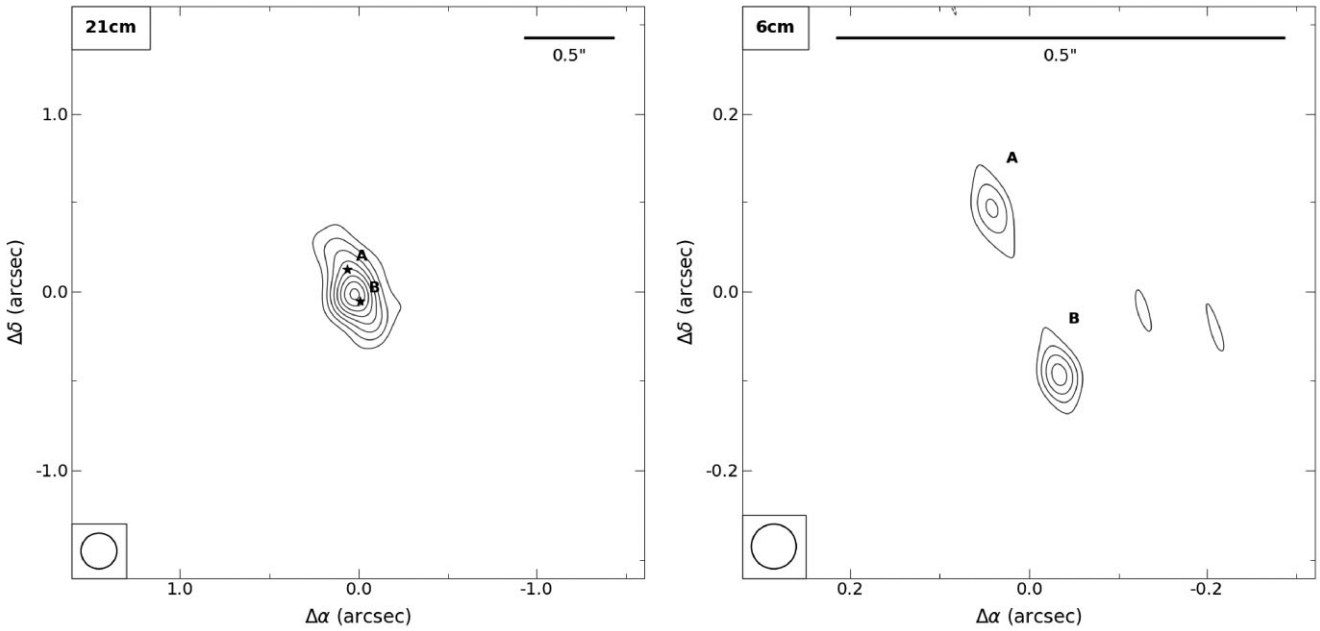

Figure 2. Contour images of the combined *L*-band and *C*-band e-MERLIN imaging. Contours for the 6 cm map are given at -3σ, 3σ, 5σ, 7σ,..., where σ is the rms noise in the map. Contours for the 21 cm map are instead given at -5σ, 5σ, 7σ, 9σ,..., where σ is the rms noise in the map. The σ values are 22.6 and 8.7 μJy beam^{-1} for the 21 and 6 cm map, respectively. A to-scale version of the circular *restoring* beam used to create each map is given in the bottom left-hand corner; the FWHM sizes are 0.2 and 0.05 arcsec for the 21 and 6 cm map, respectively. The actual *clean* beam FWHM dimensions are 0.37 and 0.13 arcsec for the major and minor axes at the *L* band. The same dimensions at the *C* band are 0.16 and 0.03 arcsec. The target is detected quite strongly in the 21 cm imaging. A weak detection of two unresolved radio sources is made in the 6 cm imaging with angular separation 0.19 ± 0.06 arcsec and PA $22^\circ \pm 10^\circ$. Both images have been cleaned to three times the theoretical noise limit.

limit for each radio source is simpler, though again limited, in its interpretation. We calculate $T_{\rm NE} > 1246$ K and $T_{\rm SW} > 1713$ K using the 0.05 arcsec circular restoring beam, which only serves to rule out the presence of a region of cold thermal emission in both sources.

4 DISCUSSION

One of the conclusions of Woo et al. (2014) was that high-resolution radio observations were necessary to look for attached radio components of the dual narrow-line region (NLR), thus indicating a pair of AGNs. The discovery of these two unresolved sources of radio emission within J132323 is major evidence in favour of a binary AGN model. Fig. 3 shows the dual radio source overlaid on the *F*550*M* Hubble image. Note that the *F*550*M* data have an absolute positional error of ∼0.1 arcsec, determined through foreground star matching to the *Gaia* catalogue (Gaia Collaboration et al. 2021). The relative positions remain accurate. Given the overlap of sources A and B with the optical cores (accurate to within this absolute error), in addition to their similarity in separation and PA, it is very likely that a binary AGN is hosted by two galaxies in the late stages of a merger. Moving forward, the issues that warrant further investigation are: long-term variability in the radio emission, as the temporal sampling of all radio observations so far is quite poor; resolving the possibility of a jet–cloud interaction in one or both of sources A and B rather than an AGN; and further observations with an alternative radio observatory for deeper imaging and to overcome the severe impact of the e-MERLIN synthesized beam orientation. We discuss these issues in order.

Variability is a common indicator of an AGN (e.g. Mooley et al. 2016), though it is not possible to conduct a useful investigation

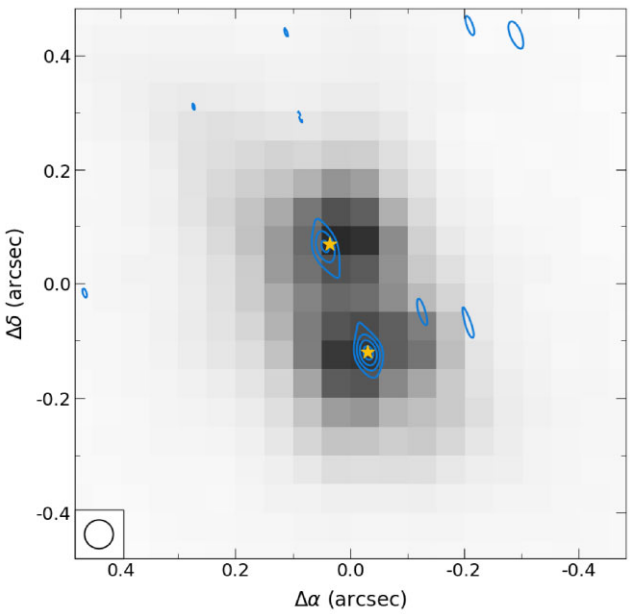

Figure 3. A plot of the *C*-band (6 cm) contours (in colour) overlaid on the *F*550*M* image (in greyscale) from the *HST*. A very small shift of ∼ pixel (corresponding to ∼0.05 arcsec) has been applied to the *F*550*M* image to bring radio source B into alignment with the brightest pixel in the south-west *F*550*M* component. Yellow markers indicating the centroids of the *HST* cores are based on the values in Woo et al. (2014). As the absolute positional information in the *HST* data is not reliable (see Section 4), we have placed the south-west marker directly over radio source B to illustrate the similarity in separation and PA.

of variability here due to the irregular spacing of epochs and their poor signal-to-noise ratio. No individual *C*-band epoch can be used for this reason. It is possible to detect A and B in the combined 2016/17 data and then again in the combined 2020 data, though the image fidelity for each epoch is significantly worse as a result of approximately halving the integration time. The *C*-band peak flux measurements for sources A and B in the 2016/17 epoch are 73 ± 14 and $101 \pm 14\,\mu\mathrm{Jy\,beam^{-1}}$, respectively. Similar measurements for the 2020 epoch are 64 ± 10 and $80 \pm 10\,\mu\mathrm{Jy\,beam^{-1}}$. These peak flux measurements are consistent within the uncertainties, so drawing any conclusions is difficult. Unfortunately, the *L*-band epochs also have their own set of problems that limit their usefulness in looking for source variability. Of the four *L*-band observations, one was conducted in late 2016, while three are conducted four years later over the space of four days. Ideally, more observations would be regularly spaced to sample any changes in accretion flow.

If, at higher resolution, only one of the two radio sources shows a core-jet morphology, the orientation of the jet could give clues as to the origin of the other source. For example, if a jet is detected in source B and it is oriented randomly and away from source A, then it is more likely that the binary AGN only displays one jet structure strong enough to be detected, and that there is in fact a black hole (BH) pair. If, however, the jet of source B is oriented towards source A, then a case might be made, depending on the structure of the emission in source A, for a jet–cloud interaction producing the dual radio structure. A binary AGN may still appear this way; it is just unlikely given the range of possible directions of the jet. This scenario would certainly require further investigation, most likely seeking deeper optical observations to look for clearer signs of a dual NLR. We note that a similar conclusion was reached in Woo et al. (2014).

Another unlikely scenario is that J132323 is actually a compact symmetric object (CSO): a very young radio source usually presenting with dual radio lobes separated by < 1 kpc (Conway 2002). These dual radio lobes often accompany a third compact radio source between them representing the central AGN. We do not expect our dual radio source to be a CSO for a few reasons; primary amongst these are the larger separation and weaker luminosity of our sources. In a young radio source, the luminosity of each lobe has a loose positive scaling with projected distance – as the jet propagates through the surrounding medium. So, one would expect that a projected separation of 1 kpc (as in the case of J132323) would be on the brighter side for a CSO. However, in a comparison with An & Baan (2012), J132323 appears to have a 1.4 GHz luminosity that is multiple orders of magnitude below even the average case of a 1 kpc CSO. In addition to this, our dual radio source is accompanied by dual stellar cores presumably associated with two distinct NLRs, whereas a CSO is, by definition, a single active BH system with two unbeamed jets. Therefore, a dual NLR system is not expected in a CSO.

Changing the weighting scheme of the e-MERLIN data does not provide any extra information. We have tested Briggs weighting with robust parameters $R \geq 0$, after which the dual radio source detection becomes lost in the noise. More information can be inferred from the relative flux density differences between the VLA and e-MERLIN data. The 6 cm flux density remains similar between the two, suggesting that the majority of this emission is compact in nature. In contrast, the 21 cm emission sees a $\sim$1 mJy increase in the VLA data, presumably because the larger VLA beam is detecting extended emission distributed throughout the discs and tails of the galaxies.

5 CONCLUSIONS

We present new e-MERLIN *C*- (6 cm) and *L*-band (21 cm) imaging of a close-separation binary AGN candidate at $z \sim 0.35$, identified by Woo et al. (2014) using *HST* imaging and VLT IFU spectra. We detect a single unresolved *L*-band source with a peak flux density of $357 \pm 22\,\mu\mathrm{Jy\,beam^{-1}}$. We also detect two unresolved *C*-band sources of similar flux density with an angular separation and PA of 0.19 ± 0.06 arcsec and $22^\circ \pm 10^\circ$, which is very similar to previous measurements of optical data representing dual cores of stellar emission. We conclude, therefore, that the target very likely harbours an active BH pair, hosted by two galaxies in the late stages of a merger. This pair is separated by 0.95 ± 0.29 kpc at the epoch of the source. To further investigate the nature of these sources, we are pursuing deeper, higher resolution observations to look for a core-jet morphology in one or both of the radio sources, to better constrain the separation and PA, and to determine a tighter constraint on the brightness temperature of the two sources. Further work may also include deeper observations in the optical and infrared band, to investigate the dynamics of the merger and the properties of the stellar populations within each galaxy.

ACKNOWLEDGEMENTS

We acknowledge use of data from e-MERLIN. e-MERLIN is a National Facility operated by the University of Manchester at Jodrell Bank Observatory on behalf of STFC, part of UK Research and Innovation. We also acknowledge use of data from the VLA operated by the National Radio Astronomy Observatory. The National Radio Astronomy Observatory is a facility of the National Science Foundation operated under cooperative agreement by Associated Universities, Inc. JEB acknowledges support in the form of a UK Science and Technology Facilities Council PhD studentship. JW acknowledges the support by the Basic Science Research Program through the National Research Foundation of Korean Government (NRF-2021R1A2C3008486). We thank the anonymous referee for useful comments that improved the paper.

DATA AVAILABILITY

The data underlying this Letter will be shared on reasonable request to the corresponding author.

REFERENCES

Albareti F. D. et al., 2017, ApJS, 233, 25
An T., Baan W. A., 2012, ApJ, 760, 77
Begelman M. C., Blandford R. D., Rees M. J., 1980, Nature, 287, 307
Bonzini M. et al., 2015, MNRAS, 453, 1079
Colpi M., 2014, Space Sci. Rev., 183, 189
Conselice C. J., 2014, ARA&A, 52, 291
Conway J. E., 2002, New Astron. Rev., 46, 263
Danzmann K. et al., 2017, LISA Laser Interferometer Space Antenna. preprint (arXiv:1702.00786)
De Rosa A. et al., 2019, New Astron. Rev., 86, 101525
Fu H., Myers A. D., Djorgovski S. G., Yan L., Wrobel J. M., Stockton A., 2015, ApJ, 799, 72
Gaia Collaboration et al., 2021, A&A, 649, A1
Goulding A. D., Pardo K., Greene J. E., Mingarelli C. M., Nyland K., Strauss M. A., 2019, ApJ, 879, L21
Hartley P., Jackson N., Sluse D., Stacey H. R., Vives-Arias H., 2019, MNRAS, 485, 3009
Högbom J. A., 1974, A&AS, 15, 417
Holley-Bockelmann K., Khan F. M., 2015, ApJ, 810, 139

Khan F. M., Just A., Merritt D., 2011, ApJ, 732, 89
Khan F. M., Holley-Bockelmann K., Berczik P., Just A., 2013, ApJ, 773, 100
Kharb P., Lal D. V., Merritt D., 2017, Nat. Astron., 1, 727
Komossa S., Zensus J. A., 2016, in Meiron Y., Li S., Liu F.-K., Spurzem R., eds, Proc. IAU Symp., Vol. 312, Star Clusters and Black Holes in Galaxies Across Cosmic Time. Cambridge Univ. Press, Cambridge, p. 13
Komossa S., Burwitz V., Hasinger G., Predehl P., Kaastra J. S., Ikebe Y., 2003, ApJ, 582, L15
Kormendy J., Ho L. C., 2013, ARA&A, 51, 511
Liu X., Greene J. E., Shen Y., Strauss M. A., 2010, ApJ, 715, 30
Manchester R. N. et al., 2013, Publ. Astron. Soc. Aust., 30, e017
Mooley K. P. et al., 2016, ApJ, 818, 105
Padovani P., 2016, A&AR, 24, 13
Padovani P., Bonzini M., Kellermann K. I., Miller N., Mainieri V., Tozzi P., 2015, MNRAS, 452, 1263
Padovani P. et al., 2017, A&AR, 25, 2
Panessa F., Baldi R. D., Laor A., Padovani P., Behar E., McHardy I., 2019, Nat. Astron., 3, 387
Rodriguez C., Taylor G. B., Zavala R. T., Peck A. B., Pollack L. K., Romani R. W., 2006, ApJ, 646, 49
Rubinur K., Das M., Kharb P., 2018, J. Astrophys. Astron., 39, 8
Vasiliev E., Antonini F., Merritt D., 2015, ApJ, 810, 49
Verbiest J. P. et al., 2016, MNRAS, 458, 1267
Woo J.-H., Cho H., Husemann B., Komossa S., Park D., Bennert V., 2014, MNRAS, 437, 32

This paper has been typeset from a TEX/LATEX file prepared by the author.